*Advanced Energy Systems and Intelligent Geoscience (AESIG)*
*https://www.mospbs.com/journal/aesig*

• *Article* •

# Zero-Shot Filling of FMI Blank Stripes Based on Deep Image Prior and an Attention-Enhanced Unet

**Yulin Du[1], Yukun Liu[1,2,*], Xiaolong Wang[1], Yiming Zhu[1], Xiang Cheng[1], Sile Wei[1]**

[1] Key Laboratory of Exploration Technologies for Oil and Gas Resources (Yangtze University), Ministry of Education, Wuhan 430100, China

[2] SINOPEC Key Laboratory of Geophysics, Nanjing 211103, China

[*]**Corresponding Author:** Yukun Liu **Email:** yukunliu@yangtzeu.edu.cn

**Received:** 01 June 2026 **Accepted:** 12 June 2026

**Abstract:** Fullbore Formation MicroImager (FMI) logging provides high-resolution electrical images of the borehole wall and has been widely used for fracture interpretation, dip analysis, and complex reservoir evaluation. However, due to limited pad coverage, borehole diameter variations, and unstable tool–wall contact, original FMI images commonly contain longitudinal blank stripes along the depth direction. These missing regions disrupt the continuity of key geological features, such as bedding interfaces, fractures, and vugs, thereby reducing the reliability of subsequent geological interpretation. Conventional methods, including inverse distance weighting and intensity-space interpolation, are computationally efficient but mainly rely on local smoothing assumptions, making them insufficient for restoring structural trends across wide missing stripes. Multiple-point geostatistical methods depend strongly on training images and may produce overly rigid texture patterns in complex heterogeneous intervals. Deep learning-based inpainting methods, particularly those based on generative adversarial networks, usually require large-scale training datasets and may introduce geologically inconsistent hallucinated details. To address these limitations, this study proposes a zero-shot FMI blank-stripe filling method based on Deep Image Prior (DIP) and an attention-enhanced U-Net embedded with Convolutional Block Attention Modules (CBAM). The proposed method requires no external training data. Instead, it uses fixed random noise as input and optimizes the CBAM-enhanced U-Net generator through masked self-supervision over valid pixels. In this way, the structural prior of the network is exploited to extend geological textures from the observed regions of the current FMI image into the blank stripes. To further alleviate brightness drift and boundary artifacts during zero-shot optimization, depth-adaptive intensity correction and Poisson blending are incorporated. In addition, a chunk-wise scheduling strategy is adopted to ensure stable restoration of long logging image sequences. Experimental results demonstrate that the proposed method improves the geometric continuity of sinusoidal bedding traces and fracture textures within blank stripes while preserving the physical intensity consistency of FMI images. Compared with conventional interpolation, multiple-point geostatistical methods, and GAN-based inpainting approaches, the proposed method is

DOI: https://doi.org/10.58244/aesig.263904

more suitable for FMI image restoration tasks that require high geological reliability.

**Keywords:** FMI logging; Blank-stripe filling; Deep image prior; U-Net; Poisson blending; Zero-shot learning

## 1 Introduction

Fullbore Formation MicroImager (FMI) logging is a key technology for characterizing complex reservoirs in oil and gas exploration and development, including fractured carbonate reservoirs and tight sandstones (Ekstrom et al., 1987; Huo et al., 2015; Pöppelreiter et al., 2010). By measuring microelectrical resistivity variations along the borehole wall, FMI logging generates high-resolution two-dimensional pseudo-color images, providing visual geological information for dip calculation, sedimentary facies analysis, and fracture identification. However, owing to the physical configuration of pad arrays and complex borehole-diameter variations, FMI tools cannot achieve complete circumferential coverage of the borehole wall. Consequently, FMI images commonly contain multiple longitudinal blank stripes, i.e., missing-data zones. These blank stripes interrupt the continuity of sinusoidal bedding traces, fracture networks, and vug boundaries, thereby interfering with manual visual interpretation and limiting subsequent machine-learning-based automatic lithofacies classification and fracture identification (Zhou et al., 2020). As illustrated in Figure 1, longitudinal blank stripes in original FMI

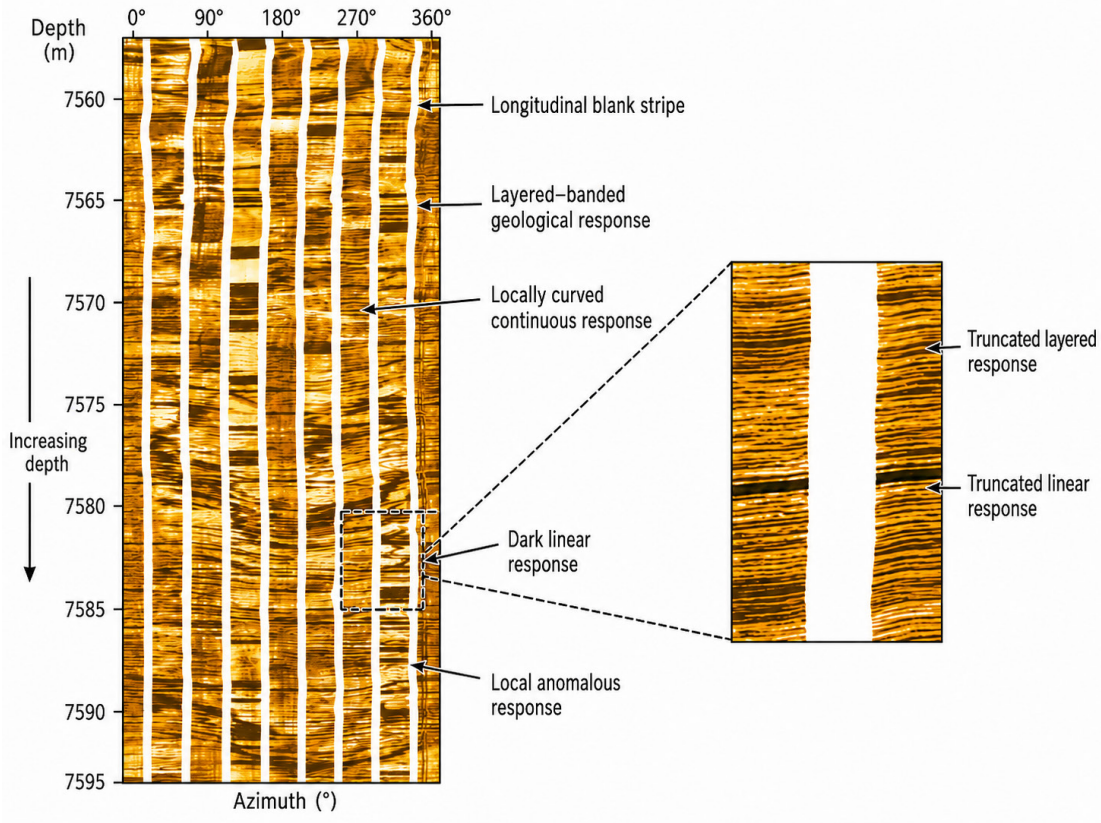


Figure 1. Longitudinal blank stripes in an original FMI image and the associated interruption of geological structures.

images may truncate layered–banded geological responses, locally curved continuous responses, dark linear responses, and local anomalous responses, thereby weakening the continuity and interpretability of key geological structures.

Several types of methods have been investigated to fill blank regions and reconstruct complete borehole-wall images. Early approaches mainly relied on purely mathematical schemes, such as inverse-distance weighting (IDW), linear interpolation, spline interpolation, and intensity-space interpolation. These methods are simple to implement and computationally efficient. However, because they infer missing pixels mainly from local spatial distances or gray-level similarity, they essentially perform smoothing-based compensation. For wide and continuous blank stripes, local interpolation tends to smooth out high-frequency fracture details and may cause originally continuous sinusoidal curves to become disconnected or misaligned within the missing regions (Hurley & Zhang, 2011).

To improve texture reconstruction, multiple-point geostatistics (MPS) has been introduced into FMI image restoration (Hurley & Zhang, 2011; Strebelle, 2002; Mariethoz & Caers, 2014). MPS extracts multipoint spatial patterns from training images and reproduces geologically plausible stochastic textures in missing regions. Nevertheless, ultradeep fault-karst carbonate reservoirs, such as those in the Shunbei area, are highly heterogeneous, with fracture, vug, and bedding textures varying substantially among different intervals (Qi, 2020a; Qi, 2020b; Jiao, 2018; Ma et al., 2022). Therefore, it is difficult to obtain a single training image that can adequately represent an entire well interval. In addition, MPS involves point-by-point scanning and pattern matching, resulting in high computational complexity and limited engineering efficiency when applied to long logging sequences.

In recent years, deep image inpainting models represented by generative adversarial networks (GANs) and context encoders have achieved strong performance in natural image completion (Pathak et al., 2016). Deep-learning methods have also been explored for borehole image-log generation and fracture detection (Zhou et al., 2020; Zhong et al., 2019). However, directly transferring these methods to logging interpretation remains challenging. First, supervised deep-learning models require a large number of paired complete-image and masked-image samples, whereas complete and missing-free training samples are difficult to obtain from real FMI data. Second, to improve visual realism, GAN-based models may generate nonexistent fractures, bedding traces, or vug boundaries in blank regions, leading to geological hallucinations. For reservoir evaluation and engineering decision-making, false fractures may cause serious misinterpretation. Therefore, FMI restoration algorithms should not only produce visually plausible results but also avoid introducing exogenous false geological information as much as possible.

To address these issues, this study proposes a zero-shot FMI blank-stripe filling method based on Deep Image Prior (DIP) and an attention-enhanced U-Net (Ulyanov et al., 2018; Ronneberger et al., 2015). The proposed method does not rely on external training datasets; instead, it directly optimizes an untrained neural network on the single FMI image to be restored. By exploiting the implicit bias of convolutional network architectures toward low-frequency structures and spatial continuity, the model can extend the geological textures of the current interval into blank stripes under valid-pixel constraints. To further enhance

structural perception, Convolutional Block Attention Modules (CBAM) are embedded into the convolutional blocks of U-Net (Woo et al., 2018). To address brightness drift and boundary stitching artifacts, depth-adaptive intensity correction and Poisson blending are introduced (Pérez et al., 2003). In addition, a chunk-wise scheduling strategy is adopted to support stable processing of long logging intervals.

## 2 Methodology and Model Architecture

The proposed method is designed to restore structured longitudinal missing regions in FMI images. The overall framework consists of five main modules: data preprocessing and mask construction, a U-Net-CBAM generator network, DIP-based zero-shot self-supervised optimization, depth-adaptive intensity correction, and Poisson blending combined with chunk-wise scheduling for long logging sequences (Ulyanov et al., 2018; Ronneberger et al., 2015; Woo et al., 2018; Pérez et al., 2003). The core idea is to exploit the neural network architecture itself as an implicit image prior, rather than learning generic restoration rules from external training data. For each data block to be restored, the network takes a fixed random-noise tensor as input and produces a completed FMI image of the same size as the original input. During optimization, the loss function is computed only over valid pixels, while the missing regions are reconstructed under the joint constraints of the network structural prior and the surrounding geological textures.

### 2.1 Data Preprocessing and Mask Construction

Let the original FMI data matrix be $Y \in R^{(H \times W)}$, where H denotes the number of samples along the depth direction and W denotes

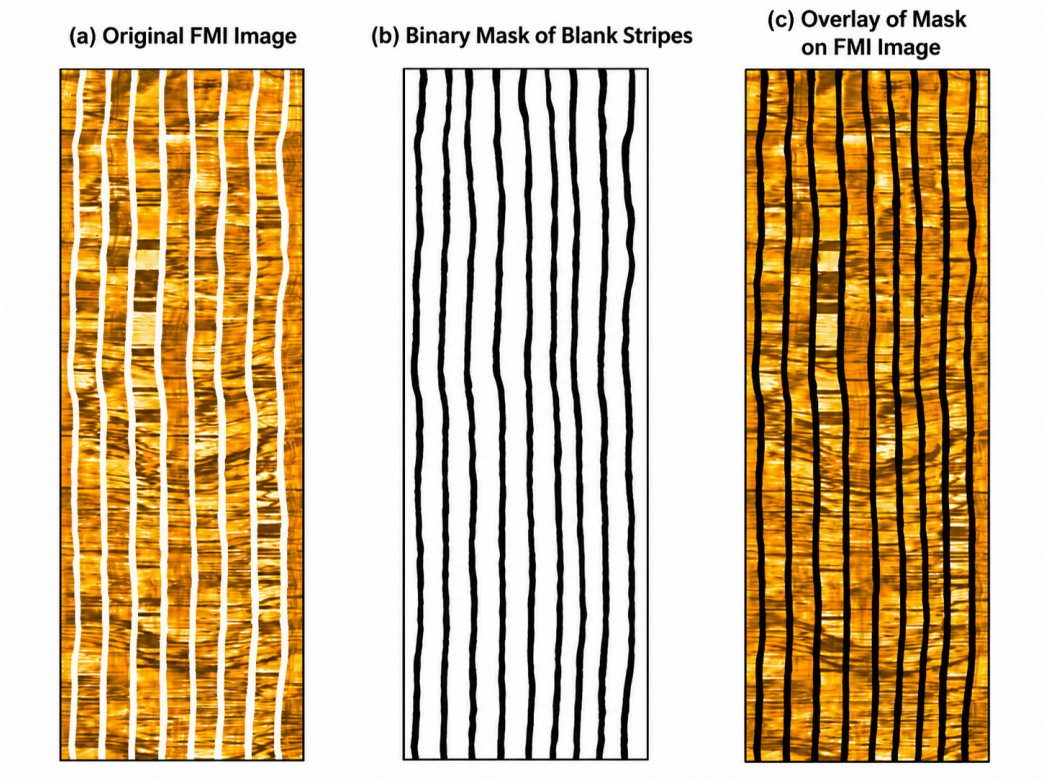


Figure 2. Original FMI image, binary blank-stripe mask, and mask overlay.

the number of samples along the azimuthal direction. Because blank stripes are commonly represented by NaN or other invalid values, a binary mask M is first generated according to pixel validity: M = 1 for valid logging responses and M = 0 for blank-stripe pixels. Considering that FMI microresistivity responses may contain local abnormally high or low values, the original data are clipped using the 1st and 99th percentiles of the valid pixels and then normalized to the interval [0, 1], so as to reduce the influence of extreme values on network optimization.

$$Y_{norm} = \frac{clip(Y, p_1\ p_{99}) - p_1}{p_{99} - p_1} \quad (1)$$

This procedure preserves the dominant texture contrast while reducing the interference of anomalous points with the self-supervised loss. For missing regions, the normalized data are temporarily filled with zeros as placeholders for tensor input. However, the loss function is not imposed on missing pixels, and therefore the network is not forced to learn erroneous zero values.

As shown in Figure 2, the original FMI image contains several longitudinal blank stripes extending along the depth direction. The corresponding binary mask clearly identifies the spatial distribution of these missing regions, and the mask overlay further verifies that the extracted blank-stripe positions are consistent with the invalid zones in the original FMI image. This mask provides the basis for subsequent masked self-supervised optimization, ensuring that the loss function is computed only over valid pixels while the missing regions are excluded from direct supervision.

## 2.2 UNet-CBAM Architecture and DIP-Based Self-Supervised Optimization

The overall workflow of the proposed zero-shot FMI blank-stripe filling method is shown in Figure 3. The original FMI image is first preprocessed to construct a binary mask that distinguishes valid logging responses from longitudinal blank stripes. A fixed random-noise tensor is then fed into the U-Net-CBAM generator network, where the encoder–decoder structure and skip connections are used to capture multiscale geological textures,

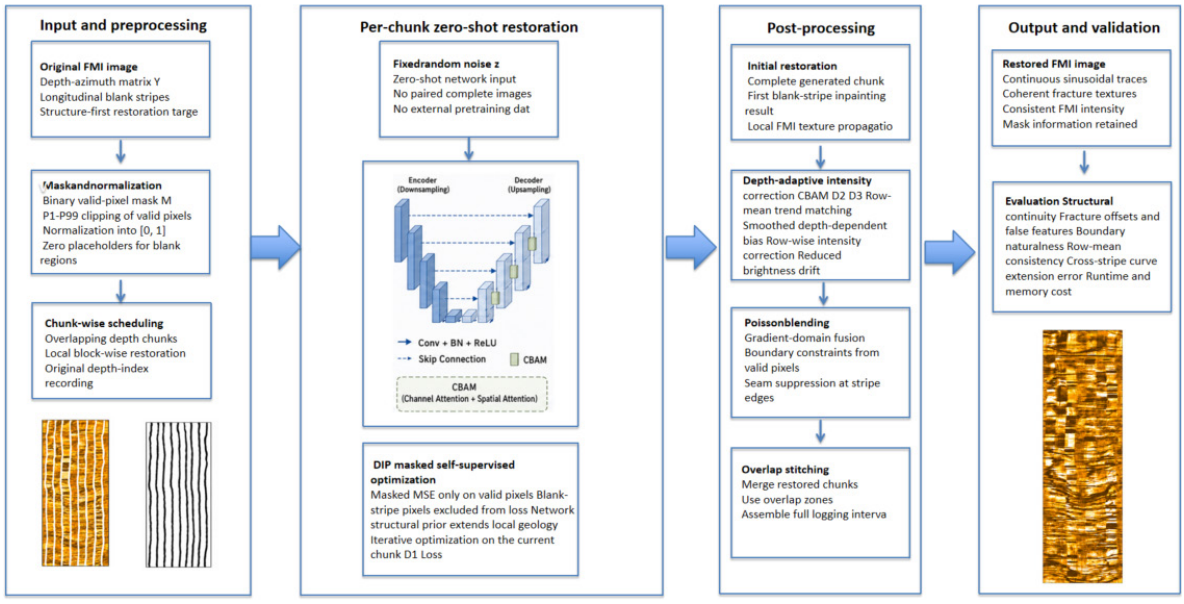


Figure 3. Overall workflow of the proposed zero-shot FMI blank-stripe filling method.

and CBAM modules are introduced to enhance feature attention along structurally important regions. During DIP-based zero-shot self-supervised optimization, the loss function is computed only over valid-pixel regions, allowing the network to infer missing stripes from the structural prior of the network itself and the surrounding geological texture constraints. The initial restoration result is further refined through depth-adaptive intensity correction and Poisson blending to improve brightness consistency and boundary smoothness. For long FMI logging sequences, a chunk-wise scheduling strategy with overlapping restoration and stitching is adopted to ensure stable full-sequence processing.

FMI images contain both macroscopic low-frequency structures and microscopic high-frequency textures (Ekstrom et al., 1987; Pöppelreiter et al., 2010). Macroscopic structures mainly appear as sinusoidal curves corresponding to bedding interfaces, faults, or fracture planes on unfolded borehole-wall images, whereas microscopic textures reflect local response differences caused by conductive fractures, dissolution vugs, and lithologic changes. To account for multiscale information, a UNet with an encoder-decoder architecture and skip connections is adopted as the generator backbone (Ronneberger et al., 2015). The encoder extracts low-dimensional semantic features layer by layer, whereas the decoder progressively restores spatial resolution. Skip connections preserve shallow texture details and are therefore favorable for extending details into missing stripes.

A Convolutional Block Attention Module (CBAM) is embedded in each convolutional block (Woo et al., 2018). CBAM consists of channel attention and spatial attention. Channel attention determines which features are more important, whereas spatial attention determines where these features should appear. For FMI blank stripes, the structural trend in the spatial dimension is particularly important because fractures and bedding traces must remain geometrically continuous across the blank zones. By adaptively weighting intermediate feature maps, CBAM enables the network to focus more strongly on sinusoidal trends, fracture orientations, and vug edges near stripe boundaries.

$$F' = M_s\left(M_c\left(F\right)\otimes F\right)\otimes\left(M_c\left(F\right)\otimes F\right) \tag{2}$$

Here, $F$ denotes the input feature map, $M_c$ denotes the channel-attention weights, $M_s$ denotes the spatial-attention weights, and $\otimes$ enotes element-wise multiplication. This module does not change the overall generation framework of UNet, but it enhances the model perception of boundaries associated with structured missing data.

The theory of Deep Image Prior suggests that the architecture of a convolutional neural network itself contains an implicit statistical preference for natural images (Ulyanov et al., 2018). Even without external training data, an untrained network fitting a single image tends to recover continuous and regular low-frequency structures earlier than random noise and disordered high-frequency anomalies. Although FMI images are not natural photographs, their bedding interfaces and fracture textures also show clear spatial continuity, and they are therefore suitable for using DIP as an implicit regularization mechanism. (Cohen et al., 2021)

Let the generator be $f_\theta$, with fixed random noise $z$ as input and restored image $f_{\theta(z)}$ as output. The training objective minimizes the mean squared error only over valid pixels; in implementation, the network parameters can be optimized using the Adam optimizer. (Kingma & Ba, 2015)

$$L\left(\theta\right) = \frac{\Sigma\left[M\odot\left(f_\theta\left(z\right)-Y_{norm}\right)^2\right]}{\Sigma M} \tag{3}$$

In this objective function, blank-stripe regions have M = 0 and do not directly participate in loss calculation. To minimize the error over valid pixels, the network must learn the observable texture distribution and structural trends of the current image and generate a spatially consistent image over the entire domain (Ulyanov et al., 2018). Accordingly, the completion of missing regions is not derived from external sample memory but from the extension of information in the current logging interval itself. Unlike GANs, the proposed method does not involve discriminator-driven competition for visual realism and does not introduce cross-well texture templates, thereby reducing the risk of geological hallucination from the underlying mechanism. (Pathak et al., 2016)

### 2.3 Post-Processing and Implementation for Long Logging Sequences

Although zero-shot DIP optimization can reconstruct structures, local brightness drift may occur in practical FMI images, especially when the missing stripe is wide or the distribution of valid pixels is uneven. In such cases, the network output in the restored area may be brighter or grayer than the surrounding formation response. Because FMI image intensity is related to microresistivity response, brightness drift may affect the interpretation of lithological boundaries and conductive fractures. Therefore, a depth-adaptive intensity correction module is designed in this study. The row-mean sequence of the original valid regions is first calculated along the depth direction, and interpolation is used to obtain a reference intensity trend over the complete depth range. Meanwhile, the row-mean sequence of the network-generated image is calculated. The difference between the two sequences forms a depth-dependent bias vector. This vector is then smoothed using a rolling window to suppress local noise and is added back to the generated image row by row, so that the background intensity of the restored region remains consistent with neighboring valid regions.

$$I_{corr}(d,x)=I_{gen}(d\ x)+smooth\left(\mu_{valid}(d)-\mu_{gen}(d)\right) \quad (4)$$

Directly replacing the blank region with the generated result may produce visible seams along blank-stripe boundaries. In FMI interpretation, boundary discontinuities not only degrade visual quality but may also interfere with subsequent automatic processing based on gradients, edges, or curve picking. Therefore, Poisson blending is introduced after intensity correction (Pérez et al., 2003). Poisson blending solves the fusion problem in the gradient domain, so that the interior of the restored region preserves the structural gradients of the generated image as much as possible while satisfying the numerical constraints of the original image at the boundary.

$$min_f \iint_\Omega |\nabla f-\nabla g| \quad s\,t \quad f=Y\ on\ \partial\Omega \quad (5)$$

The Ω denotes the blank-stripe region, ∂Ω denotes its boundary, g is the network-generated image after intensity correction, and f is the blended result. This operation substantially weakens hard boundaries between the generated and original regions and maintains continuity in both gray level and gradient.

The FMI logging data often cover intervals ranging from tens to hundreds of meters, and the number of matrix rows may reach tens of thousands or more. Feeding the entire interval into the network at once would not only impose high memory pressure but also cause the network to average local features over a large depth range, reducing its ability to fit fine fractures and local bedding details. This study therefore adopts a fixed-row chunking strategy, in which the long interval is divided into local data blocks. Each block is independently subjected to preprocessing,

DIP iterative restoration, intensity correction, and Poisson blending, and the restored blocks are then stitched according to their original depth indices.

In implementation, chunk length can be set to approximately 2000 rows, corresponding to an interval of several meters. This design makes the spatial complexity of the algorithm largely decoupled from the full logging length and provides a basis for future multi-GPU or multiprocessing acceleration. For geological interpretation, chunking also offers an additional advantage: each block mainly learns the texture distribution of a local interval, thereby reducing interference among different sedimentary facies or structural segments.

## 3 Experimental Design and Results Analysis

### 3.1 Experimental Data and Geological Background

The experiment uses FMI logging images from a representative ultradeep carbonate interval in the Shunbei oil and gas field of the Tarim Basin. These reservoirs have undergone multiple phases of tectonic deformation and dissolution, and fractures, fault planes, vugs, and bedding interfaces are well developed, resulting in strong heterogeneity. In unfolded FMI images, inclined bedding interfaces or fracture planes typically appear as sinusoidal curves with certain amplitudes and phases; conductive fractures appear as continuous or semicontinuous dark linear responses; and vugs and fractured zones may appear as local patchy anomalies.

As shown in Figure 4, the experimental FMI interval is divided into three consecutive depth sections, namely 7560–7572 m, 7572–7584 m, and 7584–7595 m, to facilitate visual comparison and subsequent restoration analysis. The original images exhibit multiple longitudinal blank stripes distributed along the depth direction, while geological responses such as layered textures,

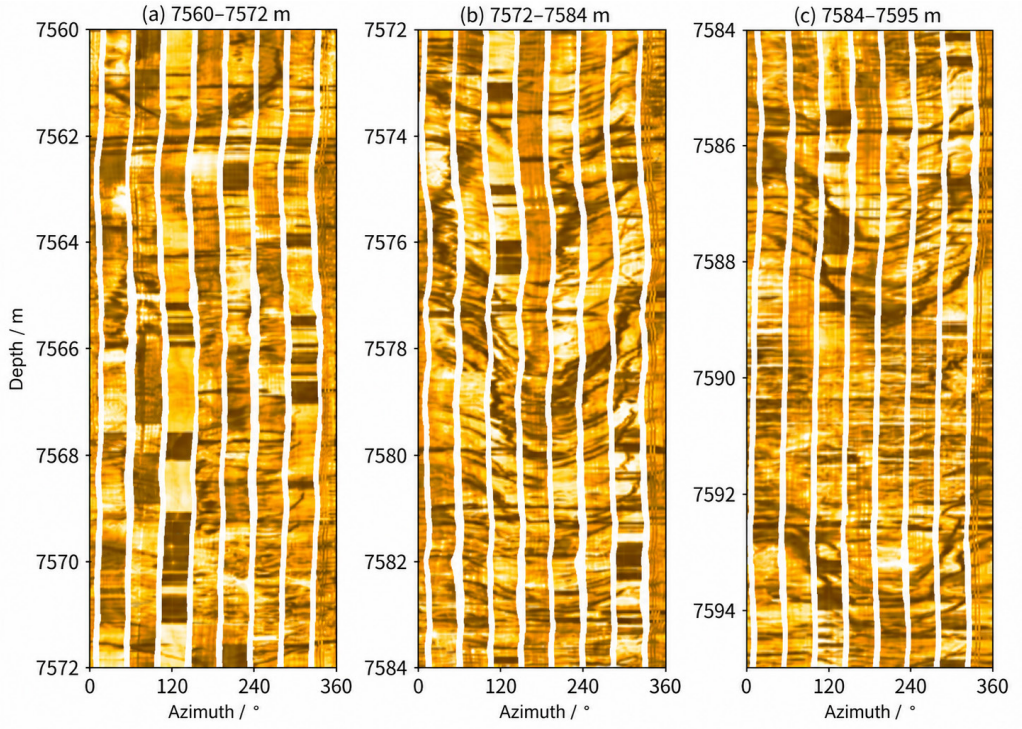


Figure 4. Original FMI images of the experimental interval and the distribution of blank stripes.

dark linear features, and local anomalous patches are developed around the missing zones. These observations indicate that the missing data are highly structured and directionally continuous, rather than randomly distributed. Therefore, restoration of this interval requires not only pixel-level completion but also the recovery of geological continuity across different azimuthal positions.

The longitudinal blank stripes in the original images are caused by structural coverage limitations of the logging tool. They usually extend along the depth direction over long distances, and their widths may reach several tens of pixels. This missing information is not random noise, but highly directional structured missing data. Unlike random occlusion in natural images, FMI blank stripes systematically interrupt all geological curves crossing the corresponding azimuthal intervals. Therefore, the objective of restoration is not simply to fill blank areas, but to recover the geological structural continuity across the stripes.

To further examine the optimization stability of the proposed zero-shot restoration framework, the training loss curves of the DIP-UNet-CBAM model were recorded for the experimental FMI interval from 7560 m to 7595 m. As shown in Figure 5, the total loss of all data blocks decreases rapidly during the early iterations and then gradually approaches a stable convergence state. This indicates that the network can quickly fit the dominant structural and textural information in the valid FMI regions under the masked self-supervised constraint. The loss curves of the four sub-intervals show similar decreasing trends, suggesting that the chunk-wise optimization strategy maintains relatively stable behavior across different depth sections. Although a transient fluctuation appears around the middle stage of optimization, the loss rapidly returns to a decreasing trajectory, indicating that the optimization process remains stable. The mean loss curve and the corresponding standard-deviation band further show that the convergence behavior among different sub-intervals is generally consistent. The decomposition of the loss components shows that the MSE loss decreases continuously with increasing iterations, while the TV loss remains within a small numerical range. This suggests that the model mainly improves data fidelity over valid pixels while maintaining spatial regularity in the restored regions. For the representative sub-interval, the lowest total loss is obtained at the final iteration, indicating that the selected iteration number is sufficient for the present experimental interval. These results support the feasibility of using DIP-based zero-shot optimization for long FMI blank-stripe filling.

### 3.2 Comparative Results and Evaluation

To evaluate the restoration performance of different methods, three representative comparison methods, namely inverse-distance weighting (IDW) interpolation, multiple-point geostatistics (MPS), and GAN-based inpainting, are selected for visual comparison with the proposed method. As shown in Figure 5, inverse-distance weighting (IDW) interpolation produces a visually continuous restored image, but the restored textures are strongly smoothed. This is because IDW mainly relies on local spatial proximity and assumes that neighboring pixels have similar responses. When the missing stripes are wide or when inclined fractures and sinusoidal bedding traces cross the missing regions, IDW cannot effectively infer the global structural trend. As a result, the restored areas tend to exhibit blurred gray-level transitions, and the original geological morphology is not truly reconstructed. Compared with IDW, multiple-point

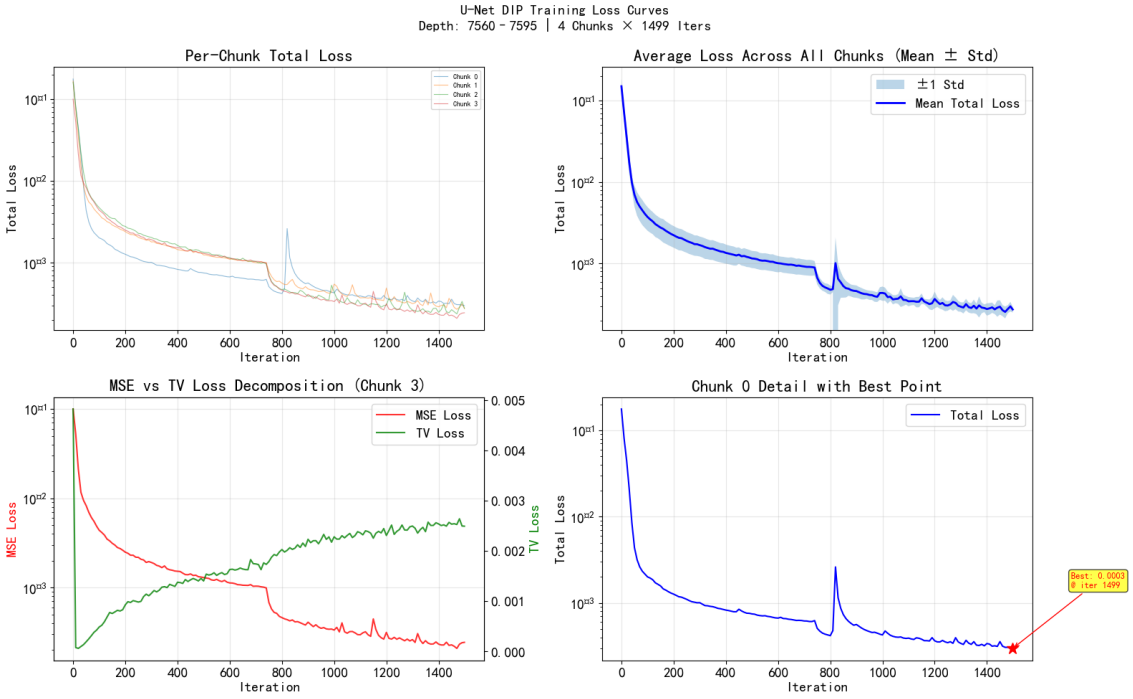


Figure 5. Training loss curves of the proposed DIP-UNet-CBAM model for the experimental FMI interval.

geostatistics (MPS) preserves more local texture variations. However, its restoration result shows obvious blocky and mosaic-like artifacts. This indicates that the reconstructed textures are strongly influenced by the selected training patterns and may not adapt well to the highly heterogeneous geological responses of the target interval. In particular, when the structural phases on both sides of a blank stripe are inconsistent, MPS may fail to maintain the continuity of sinusoidal bedding traces and fracture-related linear responses. The GAN-based result presents finer visual details than IDW and MPS, but it also introduces several artificial linear features that are not clearly supported by the surrounding FMI responses. Although these generated details may improve visual realism, they increase the risk of geological hallucination. In FMI interpretation, such false fractures or artificial boundaries may lead to misleading fracture identification and reservoir evaluation. Therefore, visual sharpness alone is insufficient for evaluating FMI image restoration; geological consistency and structural reliability should be considered more important criteria.

The restoration results indicate that the proposed method has three main advantages. First, at the macroscopic structural level, sinusoidal curves interrupted by blank stripes are naturally extended along the trends observed on both sides, and the phase and dip variations in the missing zones are smoother, reducing the horizontal smearing commonly observed in traditional interpolation. Second, at the microscopic texture level, the skip connections of UNet and the CBAM attention mechanism allow the model to preserve part of the high-frequency fracture texture, preventing excessive smoothing in the restored regions. Third, in terms of intensity consistency, the depth-adaptive correction aligns the background gray level of restored regions with neighboring regions at the same depth, avoiding overly bright or gray DIP outputs.

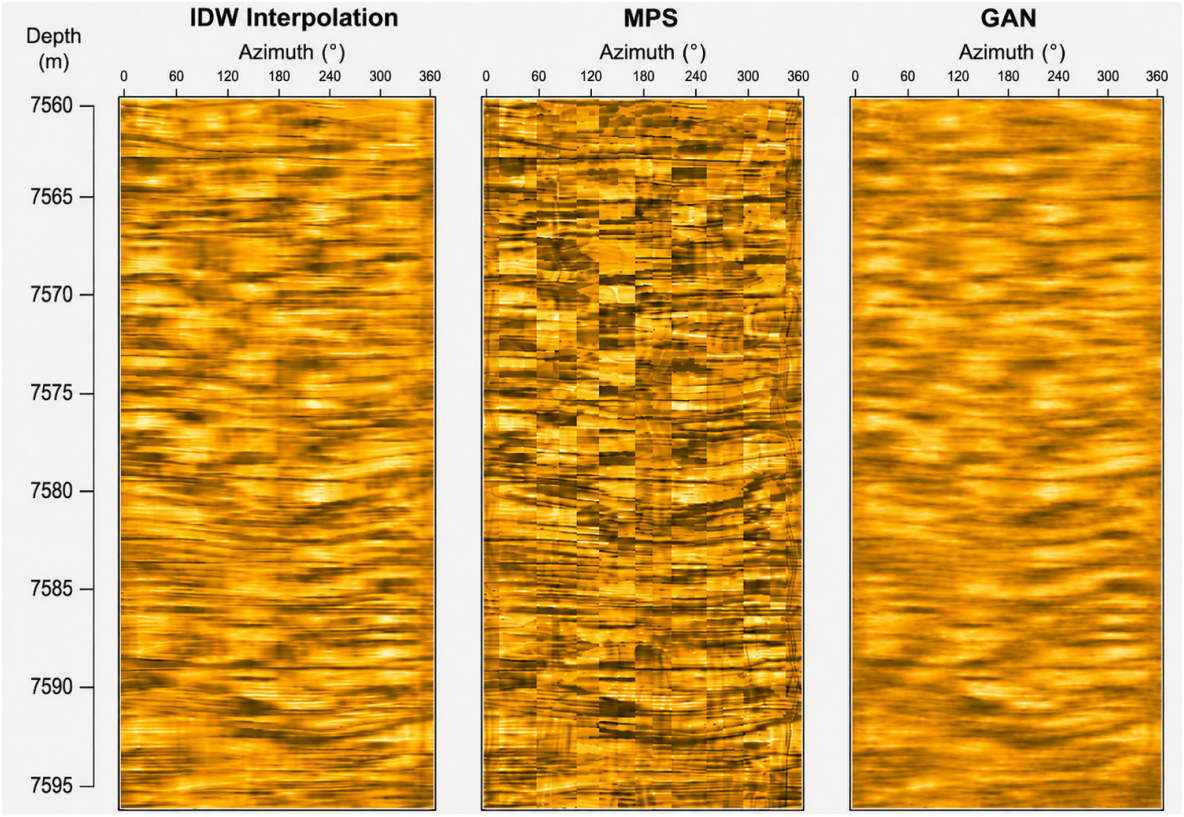


Figure 6. Comparison of blank-stripe filling results obtained by IDW, MPS, and GAN.

In particular, for fractures and bedding interfaces crossing wide blank stripes, the completion results of the proposed method better satisfy the interpretation requirement of structure-first restoration. Rather than merely pursuing local pixel similarity, the method integrates trend information from both sides of the stripe through the network receptive field and spatial attention, thereby forming more continuous geometry in the missing region. Poisson blending further removes boundary jumps between restored and original regions, making the image more stable for visual interpretation and subsequent automatic processing.

After analyzing the limitations of the comparison methods, the restoration performance of the proposed method is further examined on the same experimental FMI interval. The purpose is to evaluate whether the proposed method can better preserve geological structural continuity and intensity consistency in longitudinal blank-stripe regions. Figure 6 presents the segmented restoration results of the proposed zero-shot FMI blank-stripe filling method. The upper row shows the original FMI images and the distribution of longitudinal blank stripes in three consecutive depth intervals. These blank stripes extend continuously along the depth direction and interrupt geological responses at different azimuthal positions. The middle row shows the corresponding restoration results obtained by the proposed method. Compared with the original images, the restored results no longer contain obvious longitudinal missing zones, and the overall FMI texture remains consistent with the surrounding valid regions. The red and blue dashed boxes mark

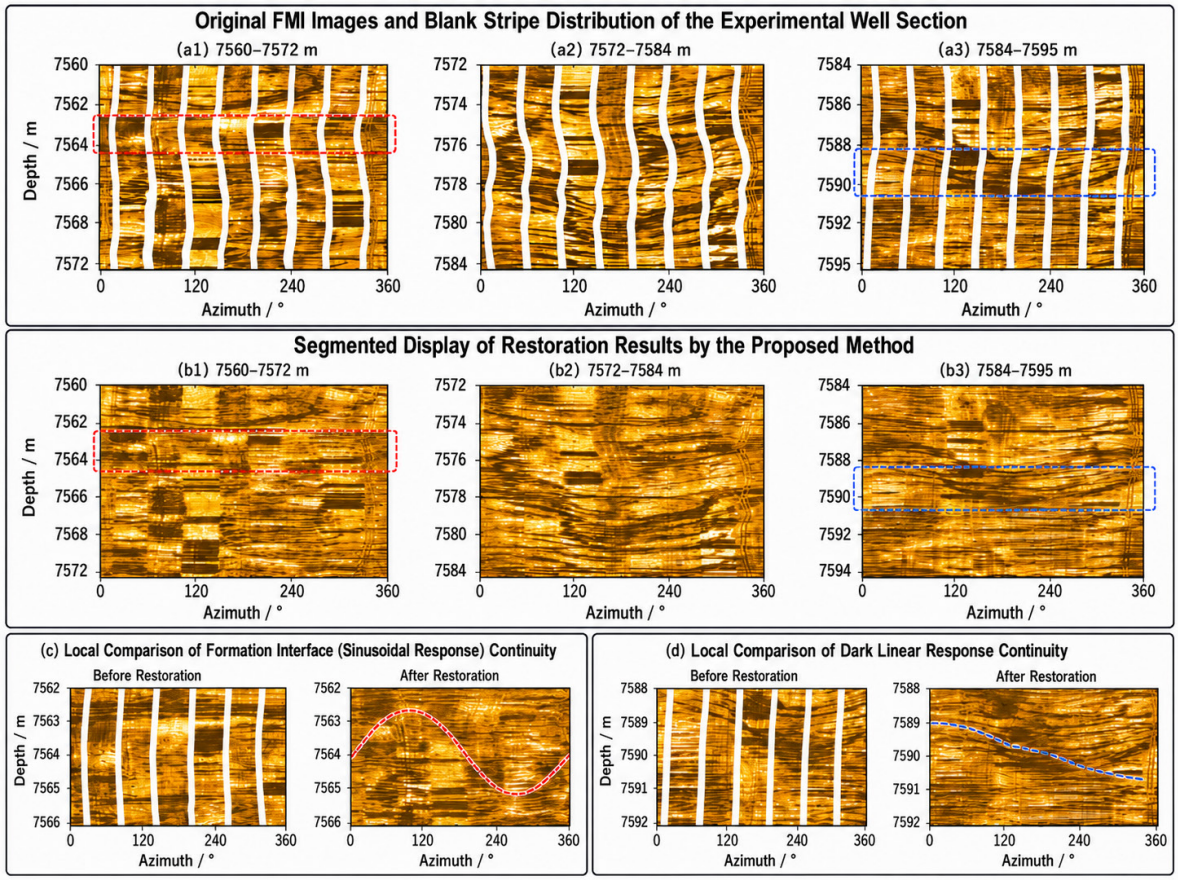


Figure 7. Local comparison before and after restoration by the proposed method: sinusoidal-curve and fracture continuity.

two representative intervals selected for detailed structural comparison. The lower row further enlarges these regions to evaluate whether key geological features are continuously reconstructed across the former blank stripes. In the local comparison of the formation interface, the sinusoidal response is clearly interrupted before restoration, whereas after restoration the curved interface can be traced more continuously across the azimuthal direction. This indicates that the proposed method can preserve the phase variation and geometric morphology of bedding-related sinusoidal traces. In the local comparison of the dark linear response, the linear geological feature is truncated by blank stripes in the original image, while the restored result shows a smoother and more coherent extension of the dark response across the missing regions. Overall, Figure7 demonstrates that the proposed method does not merely fill blank pixels, but improves the interpretability of FMI images by reconstructing the continuity of geological structures. The restored results maintain the general texture characteristics of the original FMI images, reduce discontinuities caused by blank stripes, and provide more complete image information for subsequent visual interpretation, fracture identification, and structural analysis.

Because no complete ground-truth image is available for real FMI blank-stripe regions, restoration performance is analyzed using a combination of qualitative evaluation and semi-quantitative indicators. The qualitative eval-

uation focuses on interpretation-related geological features, including whether sinusoidal bedding curves are continuous, whether fractures show obvious offsets, whether false highly conductive linear features are introduced in restored regions, whether seams occur along boundaries, and whether the background intensity is consistent with neighboring regions at the same depth.

Semi-quantitative evaluation can be conducted from the following perspectives. First, boundary gray-level jump can be measured by calculating the mean and gradient differences within a specified window on both sides of the blank-stripe boundary, thereby quantifying blending naturalness. Second, row-mean consistency can be assessed by comparing the depth-wise intensity trend of the restored image with that of the original valid regions. Third, structural continuity can be evaluated by calculating cross-stripe extension errors for manually picked or automatically detected fracture and bedding curves. Fourth, computational efficiency can be assessed by recording runtime and memory consumption under different interval lengths and chunk sizes.

### 3.3 Ablation Experiment Design and Module Contribution Analysis

To verify the contribution of each component in the proposed restoration framework, ablation experiments were conducted by removing CBAM, depth-adaptive intensity correction, and Poisson blending, respectively. The full method was also included as a reference for comparison. As shown in Figure 8, the version without CBAM can still generate a generally continuous FMI image, but the restored geological textures are relatively less organized. Some fracture-related linear responses and curved bedding features become weakened or locally discontinuous, indicating that the attention mechanism contributes to enhancing structural perception near blank-stripe regions. When depth-adaptive intensity correction is removed, obvious intensity inconsistency appears in the restored image. In particular, some regions become over-bright or show background intensity drift, suggesting that direct DIP optimization may not fully preserve the physical intensity distribution of FMI responses along the depth direction. For the version without Poisson blending, the main

Table 1. Applicability comparison of different FMI blank-stripe filling methods.

| Method | Data dependence | Structural continuity | Boundary naturalness | Engineering applicability | Main limitations |
|---|---|---|---|---|---|
| IDW / intensity-space interpolation | No training data required | Weak structural continuity | Moderate; stripe blurring | Fast and simple | Gray-level recovery only; poor geological continuity |
| MPS | High-quality training images | Moderate texture reproduction | Moderate; patchwork artifacts | Time-consuming for long intervals | Training-image dependence; limited adaptability |
| GAN-based restoration models | Paired /similar-domain samples | Visually strong but unstable | Relatively good | High training cost | Domain-shift risk; geological inconsistency |
| Proposed method (DIP-UNet-CBAM) | No external pretraining data | Strong self-supervised structural propagation | Strong boundary blending | Long-interval processing after chunking | Iterative optimization; speed–performance trade-off |

geological structures are largely retained, but boundary discontinuities and stripe-like transition artifacts remain visible near the interfaces between restored and original regions. This confirms the importance of gradient-domain blending in reducing boundary seams.

Compared with the ablated versions, the full method achieves a better balance among structural continuity, texture preservation, and intensity consistency. The restored sinusoidal bedding traces and fracture-related responses are more naturally connected across the missing stripes, while the background intensity is more consistent with neighboring valid regions. These results demonstrate that the proposed method is not merely a single network-structure modification, but an integrated restoration framework composed of network structural prior, attention enhancement, depth-adaptive intensity correction, and Poisson blending.

## 4 Discussion

The primary advantage of the proposed method lies in its zero-shot restoration strategy. It requires neither cross-well training data nor manually constructed complete images as labels, and can be directly applied to a single FMI interval requiring restoration (Ulyanov et al., 2018; Cohen et al., 2021). This property is particularly important for logging data, because complete ground-truth FMI images are difficult to obtain in real field conditions. In addition, lithological and

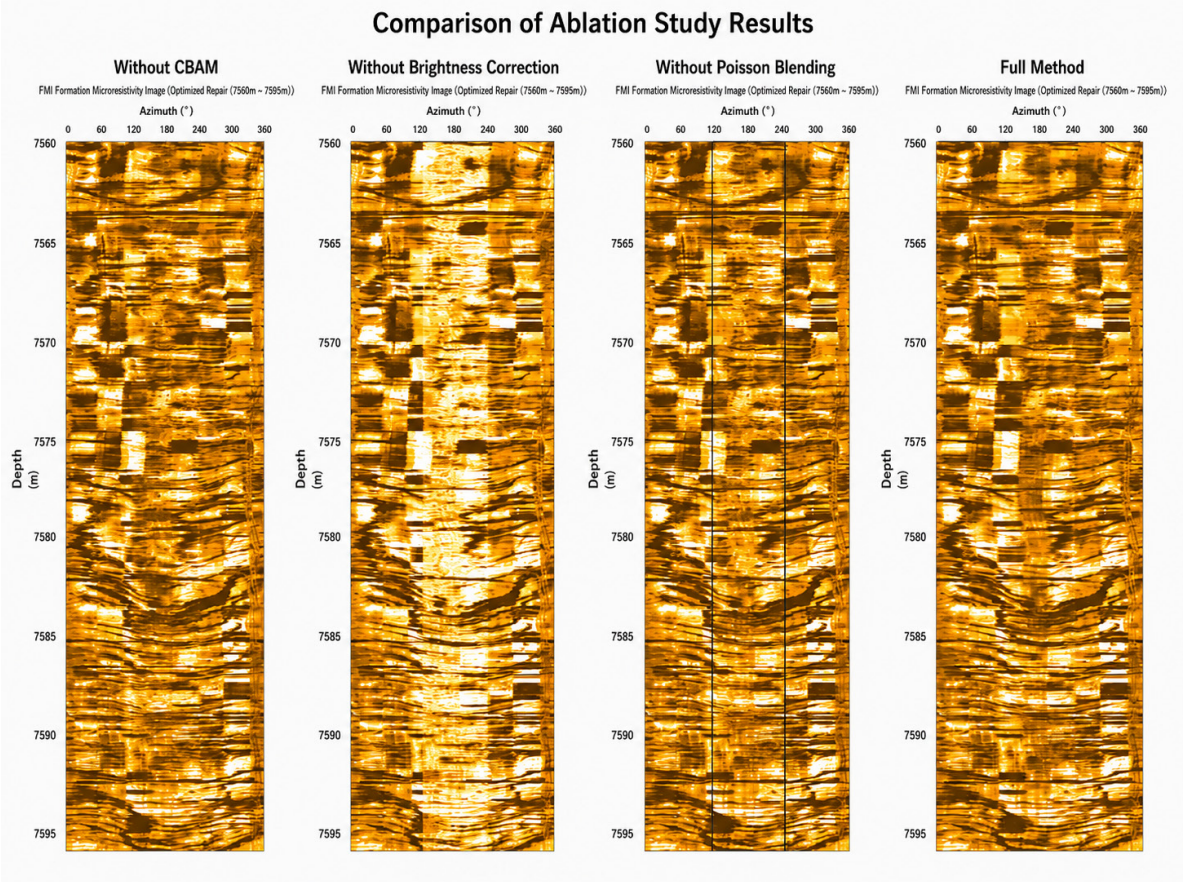


Figure 8. Ablation comparison of the proposed FMI blank-stripe filling method under four configurations: without CBAM, without depth-adaptive intensity correction, without Poisson blending, and the complete method.

structural differences among wells may lead to significant domain shifts in supervised models, thereby reducing their generalization ability when applied to heterogeneous reservoirs. Second, the proposed method emphasizes geological structural continuity. Traditional interpolation methods mainly recover gray-level values, multiple-point geostatistics mainly reproduces texture patterns from training images, and GAN-based methods mainly pursue visual realism. In contrast, FMI interpretation is primarily concerned with whether fractures, bedding traces, and geological discontinuities can be reliably connected across blank stripes. The DIP-UNet-CBAM framework provides a useful balance between physical consistency constraints and structural extension by using only the current FMI interval as the information source. This design reduces the dependence on external image libraries and helps avoid introducing cross-well textures that may not correspond to the target interval. Third, the proposed post-processing strategy considers both physical intensity consistency and boundary naturalness. Depth-adaptive intensity correction aligns the depth-wise background response of the restored regions with that of the original valid pixels, while Poisson blending suppresses stitching artifacts in the gradient domain (Pérez et al., 2003). Therefore, the final restored image is not only visually smoother but also more consistent with the physical meaning of FMI electrical responses. This is important because FMI images are not ordinary visual images; their intensity variations are related to borehole-wall electrical responses and should not be modified only for visual enhancement.

Nevertheless, the proposed method still has certain limitations. First, DIP requires iterative optimization for each data block, and its runtime is generally longer than that of supervised models using one-pass forward inference. Although the chunk-wise scheduling strategy reduces memory pressure and improves the feasibility of long-interval processing, the overall processing time is still related to the number of iterations, the blank-stripe width, and the length of the logging interval. Therefore, further acceleration strategies are needed if the method is to be applied to large-scale field datasets. Second, when a blank stripe is excessively wide and valid information on both sides is insufficient, no method relying only on the current image can fully determine the true geological structure. In such cases, the proposed method can only provide a reasonable estimate consistent with the statistical patterns and structural trends of the surrounding textures. Therefore, the restored results should be interpreted as auxiliary enhanced images rather than direct replacements for measured FMI responses. This is especially important in intervals where key fractures or vug boundaries are located mainly inside the missing regions. Third, if the valid regions of the original image contain strong noise, tool-related artifacts, or abnormal responses unrelated to geology, DIP may gradually fit these non-geological components during later optimization. This problem is related to the fitting behavior of deep image prior models, in which regular structures are usually recovered earlier than random noise, while excessive iterations may lead to overfitting. Therefore, the number of iterations should be controlled appropriately, and the restoration result corresponding to the best structural continuity and intensity consistency should be retained.

In addition, the present study mainly evaluates restoration performance based on visual interpretation, structural continuity, and intensity consistency. Future work should conduct more

systematic quantitative validation by incorporating manual interpretation results, fracture-picking results, and dip-calculation outputs. For example, the continuity of automatically picked sinusoidal curves, the stability of dip results, and the statistical differences in fracture parameters before and after restoration can be compared to further evaluate the effectiveness of the proposed method from an interpretation-task perspective. For practical applications, the chunk size should be determined according to the logging sampling rate, texture complexity, blank-stripe width, and available memory. For intervals with rapidly changing textures and dense fractures, a smaller chunk length can be used to improve local adaptability. For intervals with relatively stable textures, the chunk length can be increased appropriately to improve computational efficiency. In addition, the number of iterations should be selected according to the blank-stripe width and noise level. Too few iterations may lead to insufficient structural extension, whereas too many iterations may cause noise fitting or artificial texture enhancement. For deliverable products, the proposed method should be used as a data-enhancement step before FMI interpretation rather than as a replacement for the original data. In final figures and interpretation workflows, restored regions should be clearly marked or mask information should be preserved, so that interpreters can distinguish measured responses from algorithmically completed responses. This practice improves image completeness while maintaining the traceability of logging interpretation and reducing the risk of overinterpreting restored geological features.

## 5 Conclusions

The key objective of FMI blank-stripe filling is not merely to recover pixel intensity, but to restore the geometric continuity of geological structures such as bedding interfaces, fractures, and vug boundaries (Ekstrom et al., 1987; Pöppelreiter et al., 2010). Traditional interpolation methods are prone to blurring, horizontal smearing, and morphological misalignment in wide-stripe regions and complex fracture zones (Hurley & Zhang, 2011). MPS can introduce geological textures but depends strongly on the representativeness of the training image and has limited adaptability to strongly heterogeneous intervals (Strebelle, 2002; Mariethoz & Caers, 2014). GAN-based methods are visually expressive but rely on large-scale training samples and carry a risk of geological hallucination (Pathak et al., 2016; Zhong et al., 2019). The proposed DIP-UNet-CBAM zero-shot restoration framework does not require external training data and directly performs masked self-supervised optimization on the target FMI image (Ulyanov et al., 2018; Ronneberger et al., 2015; Woo et al., 2018). Combined with depth-adaptive intensity correction, Poisson blending, and chunk-wise scheduling, the method can improve the continuity of sinusoidal geological traces and fractures while maintaining gray-level consistency and boundary naturalness (Pérez et al., 2003). The method is especially suitable for FMI image restoration in ultradeep heterogeneous carbonate intervals such as the Shunbei area. (Qi, 2020a; Qi, 2020b; Jiao, 2018; Ma et al., 2022)

## Acknowledgments

The authors would like to thank the SINOPEC Key Laboratory of Geophysics for its support.

## Funding Statement

This work was supported by the Open Fund of the SINOPEC Key Laboratory of Geophysics (Grant No. 36750000-24-FW0399-0002) and the Natural

Science Foundation of Hubei Province, China (Grant No. 2024AFB271).

## Author Contributions

All authors contributed to the study conception and design, data collection, analysis and interpretation of the results, and manuscript preparation, and take responsibility for the integrity of the work.

## Availability of Data and Materials

None.

## Conflicts of Interest

The authors declare that they have no conflicts of interest to report regarding the present study.

## References

[1] Cohen, J. P., Brooks, L., Ouyang, C. R., et al. (2021). Limits of deep image prior for anomaly detection. *Medical Imaging with Deep Learning*, 115-126.

[2] Ekstrom, M. P., Dahan, C. A., Chen, M. Y., et al. (1987). Formation imaging with microelectrical scanning arrays. *The Log Analyst, 28*(3), 294-306.

[3] Huo, Q. L., Li, J., Wang, Y. H., et al. (2015). Application and progress of FMI logging images in geological evaluation. P*rogress in Geophysics*, *30*(2), 768-774. (in Chinese)

[4] Hurley, N. F., & Zhang, T. (2011). Method to generate fullbore images using borehole images and multi-point statistics. S*PE Reservoir Evaluation & Engineering*, *14*(2), 204-214.

[5] Jiao, F. Z. (2018). Significance and prospects of the discovery of Shunbei ultradeep carbonate fault-karst oil and gas reservoirs in the Tarim Basin. *Oil & Gas Geology, 39*(2), 207-216. (in Chinese)

[6] Kingma, D. P., & Ba, J. (2015). Adam: A method for stochastic optimization. I*nternational Conference on Learning Representations*.

[7] Ma, Y. S., Cai, X. Y., Zhao, P. R., et al. (2022). Exploration and development practice and theoretical-technological progress of the Shunbei ultradeep carbonate oil and gas field in the Tarim Basin. P*etroleum Exploration and Development*, *49*(1), 1-17. (in Chinese)

[8] Mariethoz, G., & Caers, J. (2014). M*ultiple-point geostatistics: Stochastic modeling with training images*. John Wiley & Sons.

[9] Pathak, D., Krahenbuhl, P., Donahue, J., Darrell, T., & Efros, A. A. (2016). Context encoders: Feature learning by inpainting. P*roceedings of the IEEE Conference on Computer Vision and Pattern Recognition*, 2536-2544.

[10] Pérez, P., Gangnet, M., & Blake, A. (2003). Poisson image editing. A*CM SIGGRAPH*, 313-318.

[11] Pöppelreiter, M., Garcia-Carballido, M. T., & Kraaijveld, M. A. (2010). D*ipmeter and borehole image log technology*. AAPG Memoir 92.

[12] Qi, L. X. (2020a). Characteristics and implications of the Shunbei ultradeep fault-karst oil and gas reservoirs in the Tarim Basin. P*etroleum Exploration and Development*, *47*(2), 208-216. (in Chinese)

[13] Qi, L. X. (2020b). Characteristics and implications of the Shunbei ultradeep carbonate fault-karst oil reservoir in the Tarim Basin. *China Petroleum Exploration, 25*(1), 102-111. (in Chinese)

[14] Ronneberger, O., Fischer, P., & Brox, T. (2015). U-Net: Convolutional networks for biomedical image segmentation. M*ICCAI*, 234-241.

[15] Strebelle, S. (2002). Conditional simulation of complex geological structures using multiple-point statistics. M*athematical Geology*, *34*(1), 1-21.

[16] Ulyanov, D., Vedaldi, A., & Lempitsky, V. (2018). Deep Image Prior. P*roceedings of the IEEE Conference on Computer Vision and Pattern Recognition*, 9446-9454.

[17] Woo, S., Park, J., Lee, J. Y., & Kweon, I. S. (2018). CBAM: Convolutional block attention module. E*uropean Conference on Computer Vision*, 3-19.

[18] Zhong, Z., Carr, T. R., Wu, X., & Wang, G. (2019). Application of a convolutional neural network in the generation of high-resolution borehole image logs. I*nterpretation*, *7*(3), SE51-SE63.

[19] Zhou, S., Wang, H., & Chen, Y. (2020). Automated fracture detection from borehole image logs using deep learning. C*omputers & Geosciences*, 135, 104374.